

Article

# Self-Cleaning Ceramic Tiles Produced via Stable Coating of TiO<sub>2</sub> Nanoparticles

Amid Shakeri <sup>1</sup>, Darren Yip <sup>1</sup>, Maryam Badv <sup>2</sup>, Sara M. Imani <sup>2</sup>, Mehdi Sanjari <sup>3</sup> and Tohid F. Didar <sup>1,2,4,\*</sup> 

<sup>1</sup> Department of Mechanical Engineering, McMaster University, 1280 Main Street West, Hamilton, ON L8S 4L7, Canada; shakeria@mcmaster.ca (A.S.); yipdp@mcmaster.ca (D.Y.)

<sup>2</sup> School of Biomedical Engineering, McMaster University, 1280 Main Street West, Hamilton, ON L8S 4L8, Canada; badvm@mcmaster.ca (M.B.); moetakes@mcmaster.ca (S.M.I.)

<sup>3</sup> Nanophyll Inc., 175 Longwood Rd South, Hamilton, ON L8P 0A1, Canada; mehdi@nanophyll.com

<sup>4</sup> Institute for Infectious Disease Research (IIDR), McMaster University, 1280 Main Street West, Hamilton, ON L8S 4L8, Canada

\* Correspondence: didar@mcmaster.ca

Received: 17 May 2018; Accepted: 8 June 2018; Published: 13 June 2018



**Abstract:** The high photocatalytic power of TiO<sub>2</sub> nanoparticles has drawn great attention in environmental and medical applications. Coating surfaces with these particles enables us to benefit from self-cleaning properties and decomposition of pollutants. In this paper, two strategies have been introduced to coat ceramic tiles with TiO<sub>2</sub> nanoparticles, and the self-cleaning effect of the surfaces on degradation of an organic dye under ultraviolet (UV) exposure is investigated. In the first approach, a simple one-step heat treatment method is introduced for coating, and different parameters of the heat treatment process are examined. In the second method, TiO<sub>2</sub> nanoparticles are first aminosilanized using (3-Aminopropyl)triethoxysilane (APTES) treatment followed by their covalently attachment onto CO<sub>2</sub> plasma treated ceramic tiles via *N*-(3-Dimethylaminopropyl)-*N'*-ethylcarbodiimide hydrochloride (EDC) and *N*-Hydroxysuccinimide (NHS) chemistry. We monitor TiO<sub>2</sub> nanoparticle sizes throughout the coating process using dynamic light scattering (DLS) and characterize developed surfaces using X-ray photoelectron spectroscopy (XPS). Moreover, hydrophilicity of the coated surfaces is quantified using a contact angle measurement. It is shown that applying a one-step heat treatment process with the optimum temperature of 200 °C for 5 h results in successful coating of nanoparticles and rapid degradation of dye in a short time. In the second strategy, the APTES treatment creates a stable covalent coating, while the photocatalytic capability of the particles is preserved. The results show that coated ceramic tiles are capable of fully degrading the added dyes under UV exposure in less than 24 h.

**Keywords:** TiO<sub>2</sub> nanoparticles; self-cleaning; photocatalyst; heat treatment; APTES treatment

## 1. Introduction

TiO<sub>2</sub> is one of the most well-known photocatalysts, which has been widely used for photodegradation of organic compounds and decomposition of pollutants [1–3]. While TiO<sub>2</sub> with the bulk bandgap of ~3.2 eV (in anatase phase) is transparent to visible light, it could be activated under ultraviolet (UV) light illumination and create photo-generated charge carriers [4,5]. The electrons, which are excited by UV absorption, bring about reduction of oxygen molecules in air and produce superoxide radicals (O<sub>2</sub>•<sup>-</sup>). The superoxide radicals are further reduced to form hydrogen peroxide (H<sub>2</sub>O<sub>2</sub>) and subsequently hydroxyl radicals (OH•) [6–8]. On the other hand, oxidation of water molecules by electron holes at the surface of the UV excited TiO<sub>2</sub> particles can also lead to the

formation of hydroxyl radicals and hydrogen peroxide [7,9]. These reactive oxygen species can drive decomposition of organic pollutants and inactivation of micro-organisms, such as *Escherichia coli* cell [10–12].

In addition to the photochemical power, TiO<sub>2</sub> has several other advantages, such as chemical stability, nontoxicity, hydrophilicity and cost, which make it a promising candidate for many industrial and environmental applications, including air purification, water purification, and creation of self-cleaning tiles or glasses used in constructions [9,13–15]. From a biomedical perspective, photoexcited TiO<sub>2</sub> nanoparticles (NPs) have been utilized for cancer cell therapeutics [16,17], self-sterilizing of catheters [18] and antibacterial surfaces, as well as photocatalytic disinfection [19,20].

So far, various physical and chemical approaches have been employed in order to coat TiO<sub>2</sub> NPs onto different types of surfaces. One of the most commonly used coating methods is the sol-gel deposition technique, which enables a uniform thin TiO<sub>2</sub> layer on different substrates [21–24]. Applying organic and inorganic binding agents capable of creating strong adhesion of TiO<sub>2</sub> is the other widely used strategy to directly coat different substrates with pre-synthesized TiO<sub>2</sub> particles [25]. Sopyan et al. have added TiO<sub>2</sub> particles to a paint-like sol composed of fluoropolymer resin and an organotitanium coupling agent. The sol was coated onto a glass substrate and cured at 120 °C [26]. Lin et al. have coated polyvinyl chloride (PVC) polymeric substrate with TiO<sub>2</sub> particles via dip-coating the substrate into Tetrahydrofuran (THF)-PVC-TiO<sub>2</sub> suspension [27]. In this method, THF solvent can melt the PVC, providing a strong physical attachment between TiO<sub>2</sub> particles and the substrate. In another research carried out by Pal et al., TiO<sub>2</sub> particles were combined with the inorganic binder of potassium silicate, which can create chemical bonds with substrates by a silicification process, and were then applied onto the fired bricks [28].

Silanization of inorganic surfaces with (3-Aminopropyl)triethoxysilane (APTES) is a widely known procedure to functionalize the surfaces with amino terminal groups, which could then be used to anchor different biomolecules (i.e., antibodies and proteins) via creating covalent peptide bonds [29–31]. The silanization process creates self-assembled monolayers (SAMs) of desired functional groups onto the surfaces and can be performed via chemical vapor deposition [32,33], liquid phase deposition (LPD) [34] and micro-contact printing [35–37]. APTES treatment has also been applied on TiO<sub>2</sub> particles for various purposes, such as enhancement of proteins immobilization [38], preventing the UV photobleaching [39], and grafting with thermoresponsive polymers which enables TiO<sub>2</sub> particles to have self-flocculation and temperature-controlled switching photocatalytic properties [40]. However, so far, this method has not been utilized to coat construction materials, such as ceramic tiles with TiO<sub>2</sub> particles.

Heat treatment is also a determining factor in many TiO<sub>2</sub> coating techniques. It is possible to precisely control the morphology, distribution, and size of the NPs in TiO<sub>2</sub> coating via adjusting the heat treatment parameters such as temperature and time [41–43]. In addition, heat treatment method has a prominent role in doping TiO<sub>2</sub> crystal structure with different dopants such as nitrogen and carbon for the sake of photocatalytic activity [44,45].

In this paper, two different strategies were introduced to create a stable covalent coating of TiO<sub>2</sub> NPs onto ceramic tiles to induce self-cleaning capability. In the first approach, a single heat treatment step was used to make a strong physical bond between the TiO<sub>2</sub> particles and the ceramic tile. In the second procedure, we used the APTES treatment technique to functionalize TiO<sub>2</sub> particles, and then the particles were covalently bonded to CO<sub>2</sub> plasma treated ceramic tiles. In both approaches, we have shown that the photocatalytic power of particles was preserved, the coating was stable, and the surfaces were able to thoroughly degrade the dye that was used as an organic pollutant.

## 2. Materials and Methods

### 2.1. Materials

TiO<sub>2</sub> particles grade SSP-20 (Sakai Chemical Industry Co., Osaka, Japan) with a fully anatase crystal structure, a pink food dye (A Preema Quality Product, Ingredients: Sodium Chloride and E122 Carmosine), glazed ceramic tiles with the dimension of  $\sim 3 \times 3 \text{ cm}^2$  (The Home Depot, Hamilton, ON, Canada), triethylamine (Sigma-Aldrich, Oakville, ON, Canada), ammonium hydroxide (Sigma-Aldrich, Oakville, ON, Canada), APTES (Sigma Aldrich, Oakville, ON, Canada), toluene (Sigma-Aldrich, Oakville, ON, Canada), *N*-(3-Dimethylaminopropyl)-*N'*-ethylcarbodiimide hydrochloride (EDC) (Sigma-Aldrich, Oakville, ON, Canada), and *N*-Hydroxysuccinimide (NHS) (Sigma-Aldrich, Oakville, ON, Canada) were used as received.

### 2.2. Dye-Degradation Measurements

Dye-degradation experiments were conducted using a custom-made UV chamber (Figure 1). We used a 10-watts Ultraviolet (UV) lamp (Ster-L-Ray, Preheat Germicidal Ultraviolet Lamps, Atlantic Ultraviolet Corporation, Hauppauge, NY, USA) with a total UV output of 2.7 W, a length of 21 cm, and a diameter of  $\sim 1.5 \text{ cm}$ . The chamber dimensions were  $26 \times 33 \times 25 \text{ cm}^3$ , and the distance from the lamp to the samples was around 3.5 cm. The chamber was covered with an aluminum foil to enhance the reflection.

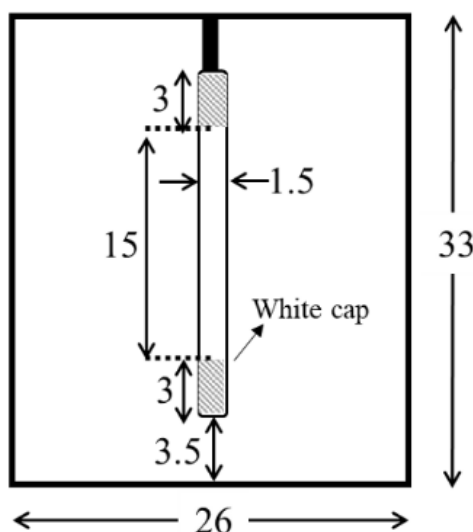


**Figure 1.** Schematic drawing of the custom-made UV chamber with a UV lamp at the center. All dimensions are in cm.

### 2.3. Dye-Degradation Measurement of TiO<sub>2</sub> Nanoparticles

The Ultraviolet-Visible (UV-VIS) spectrum of the dye was first measured to determine the optimal wavelength. This was done by using a 1.0 mg/mL concentration of the dye in deionized water and absorbances were read using a plate reader (Infinite M200 Pro, Tecan, Männedorf, Switzerland). The optimal wavelength was determined, based on results obtained using a range of excitation wavelengths. This wavelength was then used to produce a calibration curve to determine the concentration of the dye during the process of cleaning. The calibration graph was produced by measuring the absorbances for dye concentrations of 1, 0.85, 0.70, 0.55, 0.40, 0.25, and 0.1 mg/mL, respectively. Then, TiO<sub>2</sub> NPs with a concentration of 1 mg/mL in deionized water were mixed with 1 mg/mL of the coloring dye. The suspension was then kept in the UV chamber while stirring to provide consistency with the reaction. A small sample was retrieved from the reaction at 5, 15, 30,

60, 180, and 360 min, and put into a microcentrifuge tube. The tube was then spun at 14,800 rpm for 10 min to pellet the TiO<sub>2</sub> NPs out of the suspension. Next, 100 µL of the supernatant was gently pipetted from the microcentrifuge tube to the well plate. The well plate was then scanned using the plate reader, and the data obtained was graphed and interpreted.

#### 2.4. Coating TiO<sub>2</sub> Nanoparticles Using Heat Treatment Technique

Thirty microliter of 1 mg/mL TiO<sub>2</sub> NPs suspension was added onto the ceramic tiles' surfaces and spread to cover the whole surface using a simple pipetting system, and then left to dry at room temperature. The surfaces were then placed in a tube furnace or a vacuum oven for lower temperatures. The heat treatments were done in different durations of 2 h and 5 h, and at different temperatures of 100, 200, 400, 500, 700 and 900 °C. The rate of the temperature gradient in all experiments was 5 °C/min. Following heat treatment, the surfaces were rinsed and wiped to remove any unattached particle (Figure 2a). Five microliter of 1 mg/mL of dye was added onto each surface and placed in the UV chamber to evaluate the amount of dye degradation in different time intervals.

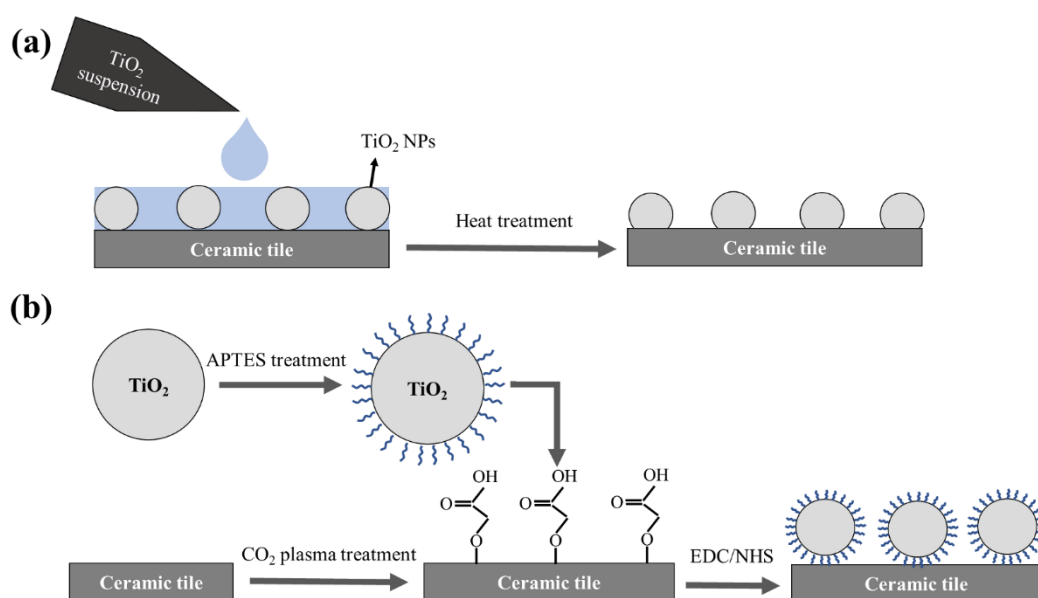


**Figure 2.** Schematic representation of (a) a heat treatment method and (b) an APTES treatment method for coating TiO<sub>2</sub> NPs on ceramic tiles.

#### 2.5. APTES Treatment Technique

TiO<sub>2</sub> NPs were homogenized with triethylamine (for improving the particle dispersion [46]) and ethanol at 60 °C. Further, ammonium hydroxide, deionized water (DI) water, and APTES (~1%) were added to the suspension and left to stir overnight. [40]. Ammonium hydroxide as a catalyst can increase the rate of APTES hydrolysis reactions [47]. Finally, the suspension was centrifuged at 4500 rpm for 15 min. The supernatant was discarded, and the pellet was mixed with ethanol. The washing step was repeated 3 times and the obtained powder was stored in 50 mL of toluene.

In order to coat ceramic tiles with the APTES treated particles, the cleaned surfaces were CO<sub>2</sub> plasma treated (Harrick Plasma, Ithaca, NY, USA) to create carboxylic groups onto the surface. EDC-NHS chemistry (a molar ratio of EDC:NHS: ~1:1) was used to activate the carboxylic groups on the surfaces. The solution was rinsed off the surface with DI water, and then the APTES treated TiO<sub>2</sub> suspension was added to the surfaces and left for 2 h. Finally, the surfaces were rinsed with DI water and dried at room temperature (Figure 2b). Five microliter of 1 mg/mL dye was added to the surfaces and left to dry. The surfaces were placed in the UV chamber and imaged at different time intervals.

## 2.6. Characterization Techniques

High-resolution XPS was used to investigate the amount of carboxylic groups induced by CO<sub>2</sub> plasma treatment of glass slides for different time durations. XPS measurements were carried out at binding energy between ~280 to ~300 (eV) to capture bond of O–C=O, C=O, C–C, and C–O as counts per second. The size distribution profile of the TiO<sub>2</sub> NPs in suspension was determined using the dynamic light scattering method (DLS, Beckman Coulter, Indianapolis, IN, USA). In DLS analysis, 10 acquisitions were performed for every experiment, and each acquisition was 15 s long. All TiO<sub>2</sub> NPs were diluted in DI water with the concentration of 0.01 mg/mL and sonicated for 5 min. For the APTES treated sample, we took 5 µL of the suspension of NPs in toluene and diluted in DI water (10 mL) to achieve the desired concentration in order to exclude the effect of toluene in DLS measurements. Contact angles were measured by an optical contact angle (OCA 35) (Future Digital Scientific Corp., Garden City, NY, USA) using 5 µL droplet of DI water. Fourier-transform infrared spectroscopy (FT-IR) (Bruker, Karlsruhe, Germany) was used to confirm the presence of the TiO<sub>2</sub> coating on the ceramic tiles' surfaces after the washing steps as well as the effect of APTES treatment on the TiO<sub>2</sub> NPs. FT-IR was conducted on different samples and different spots on the surfaces for each experiment. ImageJ was utilized to quantify the photos achieved from the dye-degradation results. For better comparison, the graphs were normalized, so that all the graphs started at the same point. Atomic force microscopy (AFM) (BioScope Catalyst, Bruker, Milton, ON, Canada) was performed to analyze surface topography and roughness within the scan size of 1 × 1 µm<sup>2</sup>. A ScanAsyst mode was utilized in the measurements using a probe with the spring constant of 0.4 N/m.

## 3. Results and Discussion

### 3.1. TiO<sub>2</sub> NPs Size Measurements

Figure 3 demonstrates the average particle sizes of untreated TiO<sub>2</sub> NPs and APTES treated TiO<sub>2</sub> NPs versus the particles population percentage. As is shown, the average radius of the untreated NPs was mostly distributed in two different sizes of 123 nm (24.3% of particle number) and 449 nm (75.7% of particle number). The existence of the larger particle sizes could be due to the NPs agglomeration even after the sonication. In Figure 3b, there were also two main particle size distributions associated with the APTES treated NPs. At the first peak, the average radius was almost the same as the untreated NPs. However, the number of NPs with that radius decreased, compared to the untreated NPs. Moreover, APTES treatment caused the second distribution to go up in terms of average radius as well as population density of the NPs. Consequently, APTES treatment of the particles caused a slight increase in the particles agglomeration, although this was not significant.

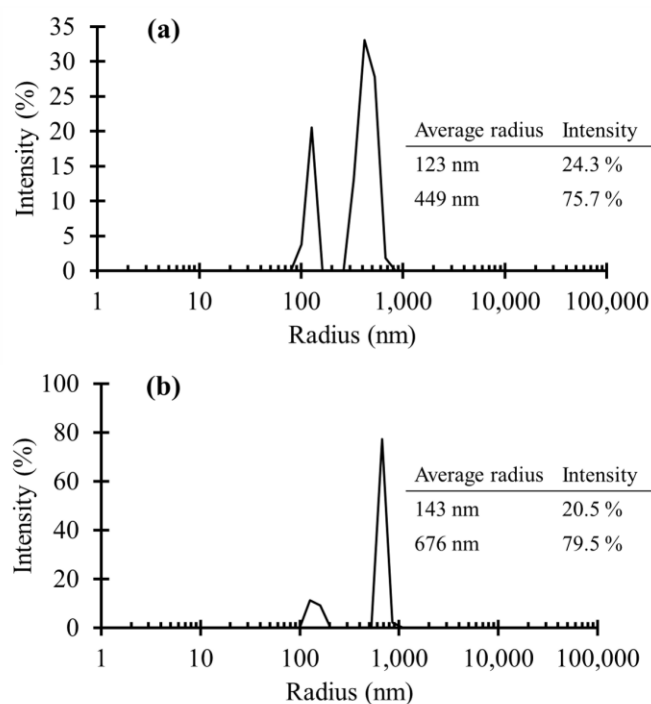


**Figure 3.** DLS results of the (a) untreated TiO<sub>2</sub> NPs and (b) APTES treated TiO<sub>2</sub> NPs. The vertical axes indicate the particle number percentages. The inset tables show the average radius of the NPs and related particle number intensities.

### 3.2. XPS Measurement of the CO<sub>2</sub> Plasma Treated Ceramic Tiles

The second approach that we employed to covalently bind TiO<sub>2</sub> NPs to the surface of ceramic tiles was aminosilanization of TiO<sub>2</sub> NPs and CO<sub>2</sub> plasma treatment of ceramic tiles. APTES treatment of TiO<sub>2</sub> NPs formed a monolayer of hydrolyzed and condensed APTES molecules on the surface providing free terminal NH<sub>2</sub> groups. Schematic presentation of this functionalization process is shown in Figure 2b. On the other hand, CO<sub>2</sub> plasma treatment of ceramic tiles can produce carboxylic groups (COOH) on the surface, which can subsequently be activated using EDC/NHS chemistry. The functional carboxylic groups can go through a chemical reaction with amino groups of the APTES treated particles and form covalent peptide bonds. Consequently, we would be able to covalently bind the TiO<sub>2</sub> particles to the ceramic tiles.

To investigate the carboxylic group formation on the surface, a high-resolution XPS test was performed. Figure 4a depicts the XPS results of an untreated sample. XPS graphs of CO<sub>2</sub> plasma treated samples for different time periods are shown in Figure 4b–d. The peaks at binding energies around 288.66 (eV), 286.02 (eV), and 284.8 (eV) were assigned to O–C=O, C=O, and C–C as well as C–O, respectively [48]. Figure 4e demonstrates the variation in the amount of O–C=O groups by increasing the CO<sub>2</sub> plasma treatment time. It could be seen that after 2 min of plasma treatment, the O–C=O band area in XPS patterns has risen from 6.46% to 16.58%, indicating the well formation of carboxylic groups via the CO<sub>2</sub> plasma treatment. Increasing the plasma treatment time more than 2 min did not significantly change the O–C=O % area.

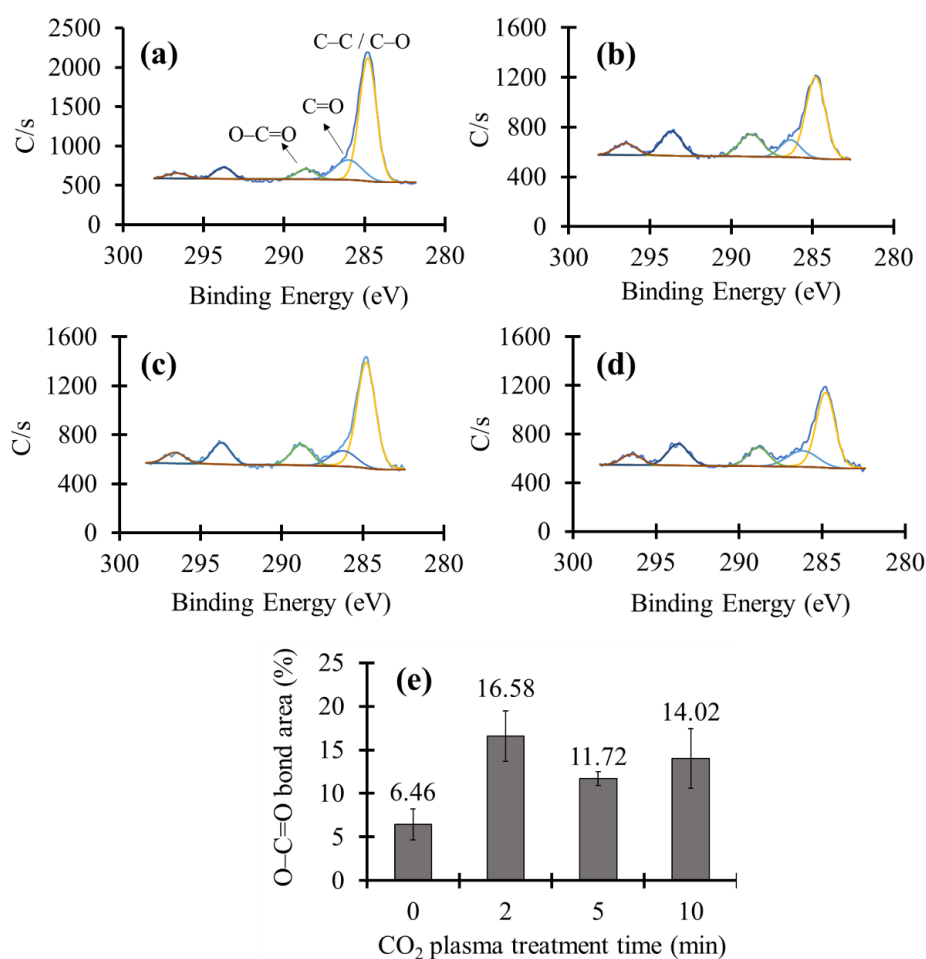


**Figure 4.** High-resolution XPS plots of CO<sub>2</sub> plasma treated glass surfaces for (a) 0 min; (b) 2 min; (c) 5 min; and (d) 10 min; (e) Variation of the amount of O-C=O bonds versus plasma treatment time.

### 3.3. FT-IR Studies of the TiO<sub>2</sub> Coated Tiles

FT-IR spectra of plain ceramic tiles, as well as the tiles coated with TiO<sub>2</sub> NPs using heat treatment and APTES treatment methods, are plotted in Figure 5. In FT-IR measurements, the surface of a plain ceramic tile was considered to be the background, and all other spectra were normalized based on that. As a control, we applied untreated TiO<sub>2</sub> NPs on ceramic tiles and then performed the regular washing steps. It can be seen that the obtained spectrum was a flat line similar to the background, indicating a complete removal of the TiO<sub>2</sub> NPs during the washing process. Nevertheless, the spectra of the TiO<sub>2</sub> coated ceramic tiles using the heat treatment protocol had a number of peaks in the absorption band between 400 to 1200 cm<sup>-1</sup>, mainly at 400 cm<sup>-1</sup>, 790 cm<sup>-1</sup>, and 900 cm<sup>-1</sup>. This absorption band could be ascribed to the Ti-O stretching and Ti-O-Ti bridging stretching modes [49–53]. Thus, the results demonstrated the presence of TiO<sub>2</sub> NPs onto the surface of the tiles after performing the washing steps. This is due to the strong adhesion of TiO<sub>2</sub> NPs to the surface induced via the heat treatment at 200 °C for 5 h (the optimum heat treatment condition based on the dye-degradation results in Figure 10). Figure 5 also depicts the same FT-IR spectra for the APTES treated NPs bonded to the plasma treated ceramic tiles. Moreover, the transmittance percentages of the peaks were almost the same as those of the heat-treated samples, which roughly illustrated the equal mass of TiO<sub>2</sub> coating. The results confirmed the stable bond formation between TiO<sub>2</sub> NPs and the substrate that retained the NPs onto the surface during the washing steps.

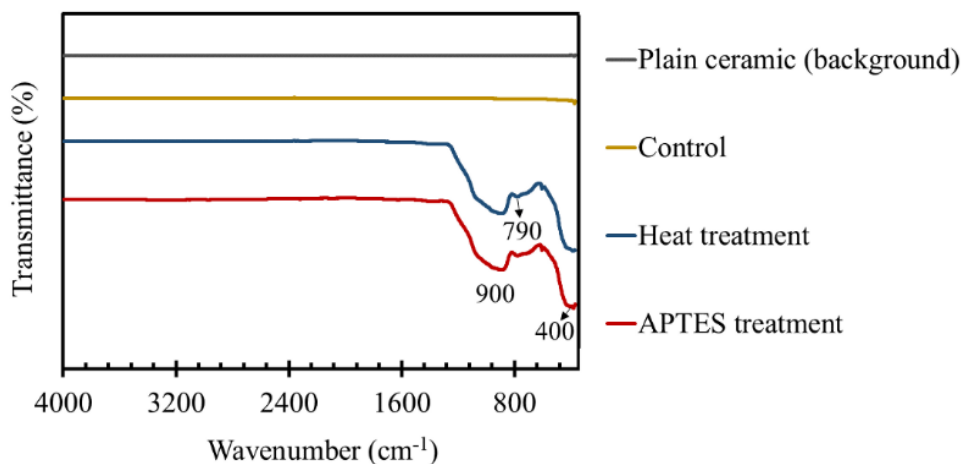


**Figure 5.** FT-IR spectra of a plain ceramic tile indicated as the background, a control ceramic tile in which untreated particles were applied to the substrate and then the washing steps were conducted, a TiO<sub>2</sub> coated ceramic tile using the heat treatment method at 200 °C for 5 h, and a TiO<sub>2</sub> coated ceramic tile using an APTES treatment protocol.

In Figure 6, the FT-IR spectra of APTES treated TiO<sub>2</sub> NPs and untreated NPs were compared at the wavenumber between 2400 to 4000 cm<sup>-1</sup> to confirm the efficacy of APTES functionalization. There are two main peaks at ~2900 and ~3300 in the transmittance spectrum of untreated TiO<sub>2</sub> NPs, which indicate the presence of hydroxyl groups on the surface of the NPs. The first peak could be associated with both symmetric and asymmetric CH<sub>2</sub> stretching vibrations in -CH<sub>2</sub>-OH compound [54], and the second peak was attributed to hydroxyl group symmetric and asymmetric stretching vibrations in Ti-OH compounds [49]. The hydroxyl groups can be formed due to the chemical and physical adsorptions of atmosphere moisture on the surface of NPs [49,55]. As shown in Figure 6, for the APTES treated particles, the peaks related to hydroxyl groups almost disappeared, and a broad peak between 2800 to 3600 cm<sup>-1</sup> was formed in the spectrum of APTES treated NPs instead. This is because of the hydrolysis and condensation reactions of the silane head groups in APTES molecules and anchoring to the hydroxyl groups of the NPs surfaces to form oxane (Si-O-M) bonds [56]. The broad peak could be caused by OH stretching in silanol (Si-OH) groups (3200–3700 cm<sup>-1</sup>) formed via hydrolysis of APTES, primary amine (3160–3450 cm<sup>-1</sup>), as well as alkane C-H stretching vibrations in -CH<sub>3</sub> and -CH<sub>2</sub>- (2840–2975 cm<sup>-1</sup>) due to the presence of APTES molecules [54].

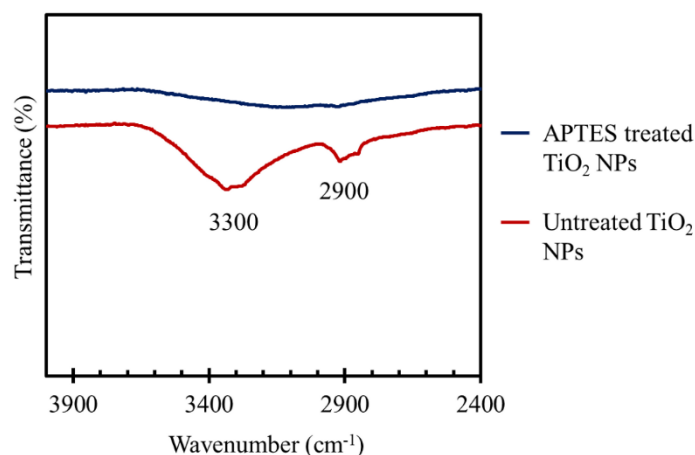


**Figure 6.** FT-IR spectra of the APTES treated TiO<sub>2</sub> NPs compared to untreated NPs at the wavenumber between 2400 to 4000 cm<sup>-1</sup>.

### 3.4. Hydrophilicity and Surface Topography of the TiO<sub>2</sub> Coated Tiles

The results of the contact angle measurement are shown in Figure 7. The contact angle of plain ceramic tiles was about  $25.8 \pm 4.0^\circ$  indicating the hydrophilic behavior of the surfaces. By performing heat treatment, although surfaces remained hydrophilic, the contact angle rose to  $77.8 \pm 3.2^\circ$ . This unexpected increase in contact angle could be due to the surface roughness generated by partial diffusion of TiO<sub>2</sub> NPs into the surface, which can compensate for the inherent hydrophilicity of TiO<sub>2</sub> [57]. The APTES treatment method, on the other hand, resulted in more hydrophilic TiO<sub>2</sub> coated surfaces with the contact angle of less than  $5^\circ$ . A possible explanation for that is CO<sub>2</sub> plasma treatment step during the APTES treatment protocol, which can greatly increase hydrophilicity as well as the APTES coating on the surface of the NPs [58].

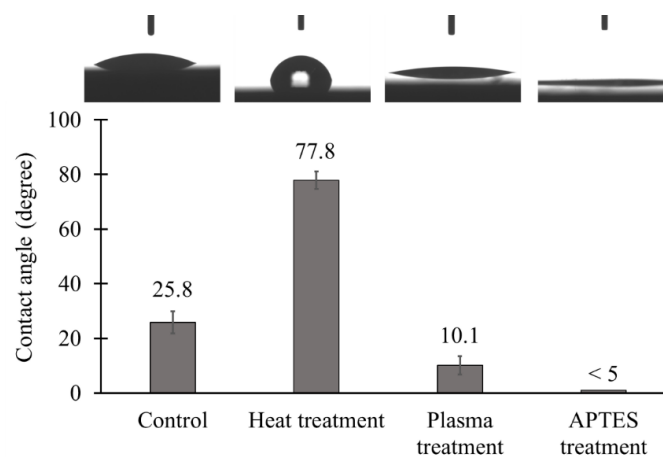


**Figure 7.** Contact angles of plain ceramic tiles (control), TiO<sub>2</sub> coated ceramic tiles via the heat treatment method at 200 °C for 5 h, CO<sub>2</sub> plasma treated ceramic tiles, and TiO<sub>2</sub> coated ceramic tiles via the APTES treatment method ( $n = 3$ ).

AFM images of the TiO<sub>2</sub> coated ceramic tiles are illustrated in Figure 8. The density of the NPs in the heat-treated sample (Figure 8a) was higher, compared to the sample coated with the APTES treatment protocol (Figure 8b). Furthermore, the root-mean-square (RMS) surface roughness of the ceramic tile increased from 0.676 nm for a plain ceramic to 1.26 nm for TiO<sub>2</sub> coated ceramic using the APTES treatment method. The RMS parameter of the TiO<sub>2</sub> coated ceramic tiles with the heat treatment process was 1.82 nm, which was more than that for tiles with the APTES treatment protocol due to the higher number of NPs on the surface.

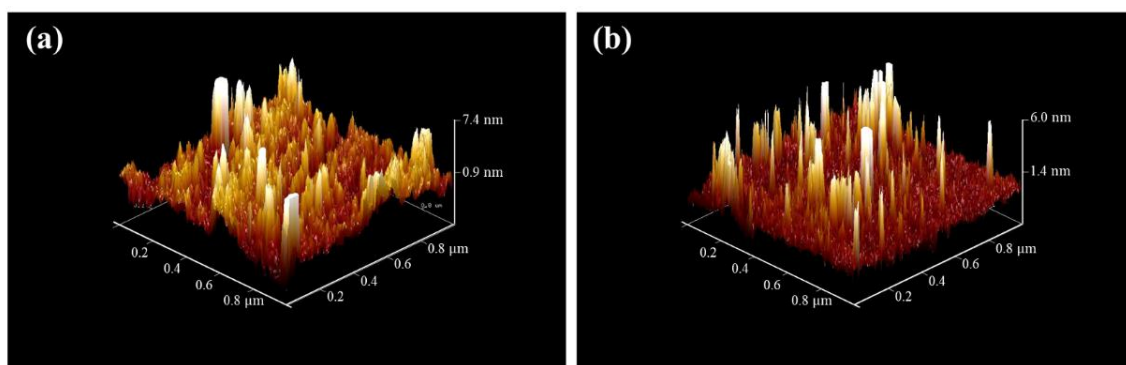


**Figure 8.** 3D AFM images of ceramic tile surfaces coated with TiO<sub>2</sub> NPs using (a) heat treatment at 200 °C for 5 h and (b) the APTES treatment method.

### 3.5. Dye Degradation of TiO<sub>2</sub> NPs in Suspension

In order to achieve the proper wavelength for reading the absorbances of the dye with a plate reader, the full absorbance spectra of 1 mg/mL concentration of the dye diluted in deionized water was measured. As shown in Figure 9a, the sharp peak at the wavelength of 512 nm, which can be easily distinguished, was used as a reference wavelength for the next absorbance measurements. The calibration curve for dye absorbance as a function of concentration at the wavelength of 512 nm is illustrated in Figure 9b. The obtained scatter diagram has a linear trend line. To measure the photocatalytic power of TiO<sub>2</sub> NPs, the particles were added to the 1 mg/mL dye solution and were kept in the UV light, under a constant stirring condition. The amount of dye-degradation induced by TiO<sub>2</sub> photocatalyst could be calculated based on Figure 9b. The dye concentration results versus UV exposure time are shown in Figure 9c. As is shown, a considerable reduction in the dye concentration was achieved after 15 min where almost half of the dye was degraded, and the concentration reached 0.55 mg/mL. Afterwards, the rate of dye degradation became slower and after 1 day of UV irradiation, the dye concentration decreased down to 0.26 mg/mL. Thus, the TiO<sub>2</sub> nanoparticles possessed a considerable photocatalytic power in suspension. The reason why the expected exponential decay to zero was not observed in our sample could be attributed to the absorption of the partial degradation products on the photocatalyst surface and/or the pH variation of the suspension leading to deterioration in the dye-degradation process.

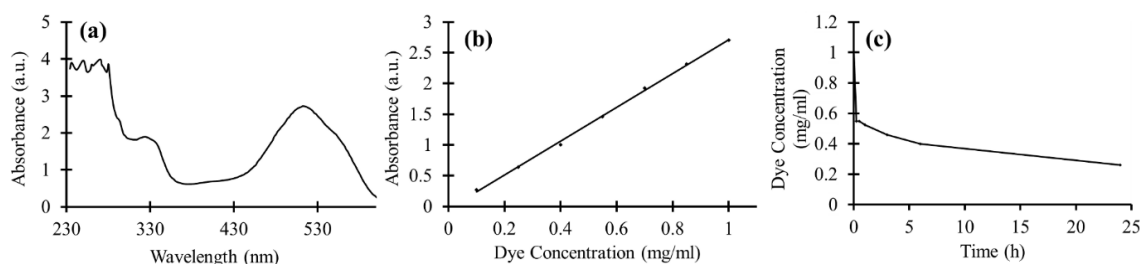


**Figure 9.** (a) UV–VIS spectra of 1 mg/mL concentration of the dye; (b) Absorbance curve as a function of dye concentration at the wavelength of 512 nm; (c) Dye concentration mixed with TiO<sub>2</sub> NPs suspension as a function of UV exposure time.

### 3.6. Dye Degradation on TiO<sub>2</sub> Coated Tiles Produced Using Heat Treatment

Figure 10 demonstrates the dye-degradation properties of ceramic tiles coated with TiO<sub>2</sub> nanoparticles using the heat treatment approach at different temperatures and incubation time (1 and 5 h). Control ceramic tiles were incubated with a suspension of TiO<sub>2</sub> NPs with the same incubation time, but no heat treatment was involved (labeled by “no heat treatment” in Figure 10). Following the washing step, all TiO<sub>2</sub> NPs were detached from the surface of control tiles and therefore, no dye degradation was observed. Moreover, when the samples were heat treated for 1 h (Figure 10a), no dye-degradation properties were recorded at any heat treatment temperatures. One major problem with high temperatures of 700 °C and 900 °C is that since the temperatures were above the phase transition temperature of TiO<sub>2</sub> from anatase to rutile [59–62], the formed rutile phase could have deteriorated the photocatalytic activity of the TiO<sub>2</sub> particles even if the particles were successfully attached to the ceramic tiles. It has been proved that TiO<sub>2</sub> exhibits a higher photocatalytic activity in anatase phase compared to fully rutile phase, which may be due to larger band gap in anatase compared to rutile TiO<sub>2</sub> [4]. Thus, the optimal temperature for heat treatment should not change the structure of TiO<sub>2</sub>. According to the composite phase diagram of TiO<sub>2</sub>, the anatase-rutile phase transition takes place at around 600 °C at atmospheric pressure [59].

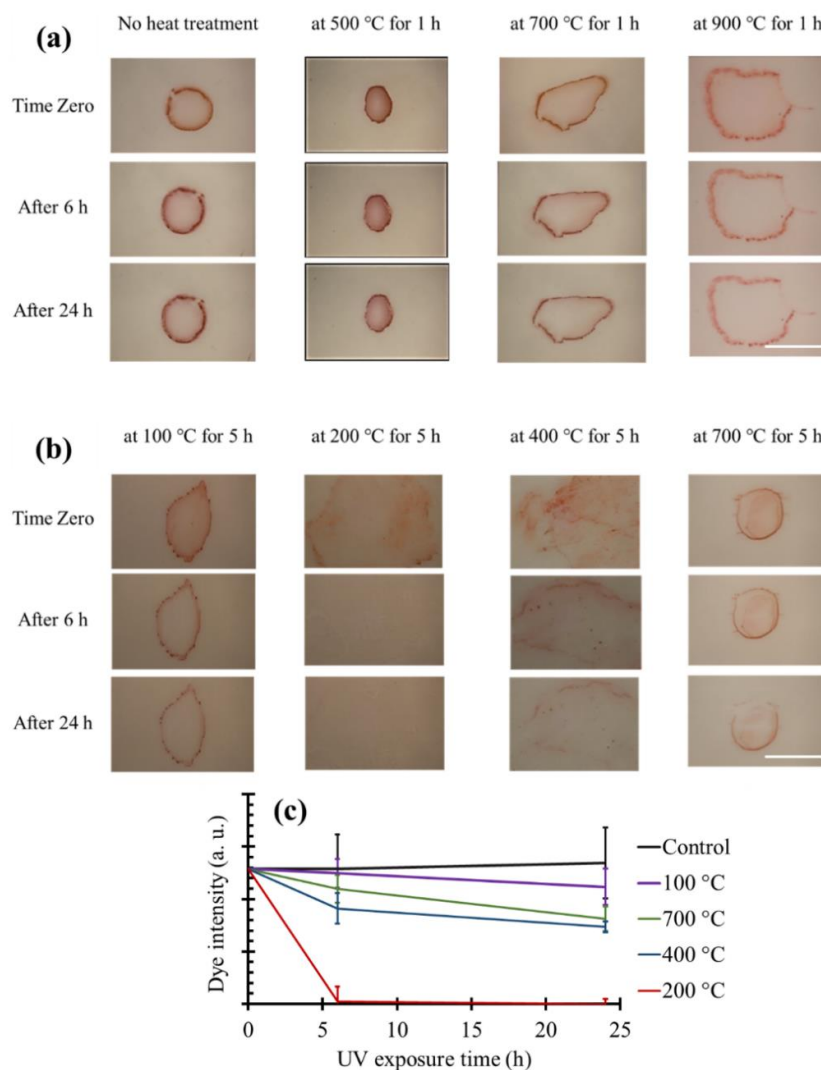


**Figure 10.** Dye-degradation results of the heat-treated ceramic tiles under UV exposure. Heat treatment was performed at different temperatures for 1 h (a) and 5 h (b). Scale bars are 1 cm. (c) Quantification of the dye degradation on the heat-treated samples for 5 h at different temperatures and the control sample without any heat treatment.

Therefore, we increased the heat treatment duration from 1 h to 5 h to investigate the effect of heat treatment time on the coating process, specially the possibility of successful and functional coating at lower temperatures. Figure 10b exhibits the dye-degradation trend for the ceramic tile samples, which were heat treated at varying temperatures for 5 h. In Figure 10c, the results were also quantified for better comparison. The samples that were heat treated at 400 °C degraded the dye at a lower rate than heat treatment at 200 °C, although both temperatures were below the anatase-rutile phase transition temperature. This can be caused by slightly more agglomeration of the TiO<sub>2</sub> NPs at 400 °C in comparison to 200 °C, leading to a small increase in the average particle size and a reduction in the overall surface area of the particles, thereby diminishing the photocatalytic power. The other possible explanation could be attributed to the higher diffusion of NPs inside the glossy surface of the ceramic tiles at 400 °C. Therefore, the smaller area of the particles would get in touch with the dye, causing a decrease in the dye-degradation rate. Performing the heat treatment at a more cost-effective temperature of 200 °C caused the dye to be fully degraded after 6 h. Nevertheless, 100 °C heat treatment for 5 h appeared to be not enough for the TiO<sub>2</sub> particles to be completely attached to the

surface of ceramic tiles, thereby resulting in less dye degradation under UV exposure. Therefore, a 5 h heat treatment at 200 °C provided the best dye-degradation properties for the ceramic tiles.

### 3.7. Dye Degradation on TiO<sub>2</sub> Coated Tiles Produced Using Aminosilanization

Figure 11a illustrates the dye-degradation results of the ceramic tiles coated with the APTES treatment method. Quantifications of the obtained results are plotted in Figure 11b. We applied untreated TiO<sub>2</sub> particles onto the ceramic tiles as control samples. Most of the particles were removed from the surface during the washing process, and the dye was not degraded after 1 day in control samples. However, when APTES treated particles were used, the dye was almost invisible after 24 h, demonstrating excellent effectivity of the APTES treatment process for coating ceramic tiles with TiO<sub>2</sub> NPs. In comparison to the heat treatment at 200 °C for 5 h, coating the surfaces via the APTES treatment resulted in a lower rate of dye degradation due to two main reasons: a smaller number of particles on the surface which was confirmed with AFM test, and covering the particles via a silane coupling agent which can reduce the photoactivity of the particles [63]. Nevertheless, using the APTES treatment protocol has two important advantages. First, the method for functionalization using APTES is much simpler and does not require high temperatures compared to the heat treatment. Second, since this technique creates covalent bonds between TiO<sub>2</sub> NPs and surfaces, the durability of the coating would be higher in the long term.

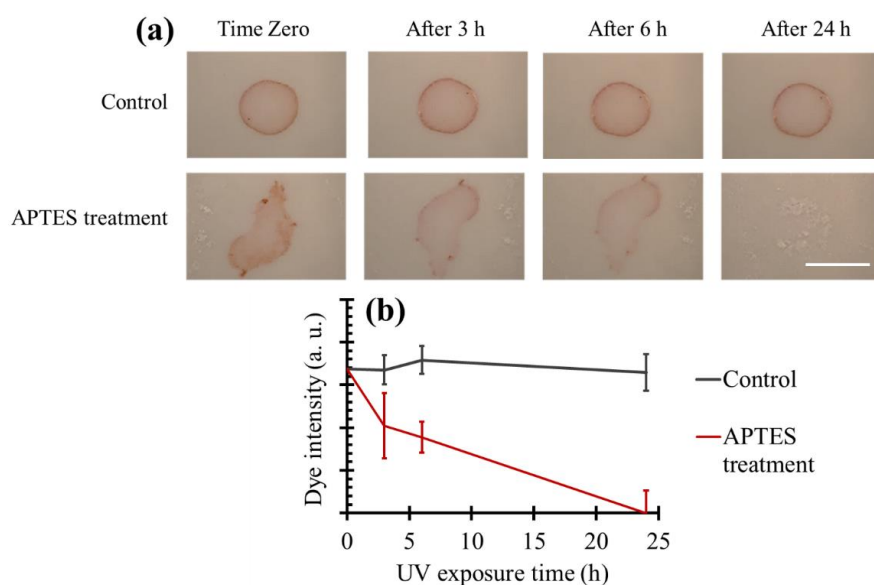


**Figure 11.** (a) Dye-degradation results of the ceramic tiles coated with TiO<sub>2</sub> particles using the APTES treatment technique. Scale bar is 1 cm. (b) Quantification of the dye-degradation images.

## 4. Conclusions

The photocatalytic power of TiO<sub>2</sub> NPs measured inside the suspension showed a proper dye-degradation effect under UV exposure. We introduced two strategies to coat ceramic tiles with the TiO<sub>2</sub> NPs. Both protocols led to transparent TiO<sub>2</sub> coating on ceramic tiles without any adverse effect on the tile's physical appearance. In the heat treatment approach, it was shown that applying a simple one-step heat treatment with the optimum temperature of 200 °C for 5 h resulted in rapid degradation of dye in a short time. In the second strategy, the APTES treatment method was employed to covalently bond the TiO<sub>2</sub> particles to the CO<sub>2</sub> treated ceramic tiles, while the photocatalytic power of the particles was preserved. The success of the covalent bonding protocol suggests a possible longer duration of the coating in harsh environments. In future, we will focus on enhancement of the self-cleaning behavior, as well as studying the durability of the coating by performing proper weathering tests.

**Author Contributions:** T.F.D. conceived the research and supervised the experiments. A.S. performed the experiments, data validation, data visualization, and analysis with help from D.Y. A.S. wrote the manuscript with input from T.F.D. and M.S. M.B. conducted the FT-IR tests. S.M.I. performed the AFM analyses. All authors have read, commented and approved the final version of the paper.

**Funding:** This project was supported by an ENGAGE-OCE-VIPI grant from the Natural Science and Engineering Research Council of Canada (NSERC, Ontario Centers of Excellence (OCE) and Nanophyll Inc.

**Conflicts of Interest:** M.S. holds equity in Nanophyll Inc.

## References

1. Dong, H.; Zeng, G.; Tang, L.; Fan, C.; Zhang, C.; He, X.; He, Y. An overview on limitations of TiO<sub>2</sub>-based particles for photocatalytic degradation of organic pollutants and the corresponding countermeasures. *Water Res.* **2015**, *79*, 128–146. [[CrossRef](#)] [[PubMed](#)]
2. Weon, S.; Kim, J.; Choi, W. Dual-components modified TiO<sub>2</sub> with Pt and fluoride as deactivation-resistant photocatalyst for the degradation of volatile organic compound. *Appl. Catal. B Environ.* **2018**, *220*, 1–8. [[CrossRef](#)]
3. Li, S.; Ishikawa, S.; Huang, C.; Zhang, W.; Tanizaki, T.; Higuchi, T.; Haraga, H. Production of active intermediates and decomposition behaviors of organic compounds in the ultraviolet ray/supersonic wave reactions with TiO<sub>2</sub> photocatalyst. *Sustain. Environ. Res.* **2015**, *25*, 67–72.
4. Luttrell, T.; Halpegamage, S.; Tao, J.; Kramer, A.; Sutter, E.; Batzill, M. Why is anatase a better photocatalyst than rutile? Model studies on epitaxial TiO<sub>2</sub> films. *Sci. Rep.* **2015**, *4*, 4043. [[CrossRef](#)] [[PubMed](#)]
5. Hashimoto, K.; Irie, H.; Fujishima, A. TiO<sub>2</sub> photocatalysis: A historical overview and future prospects. *Jpn. J. Appl. Phys.* **2005**, *44*, 8269–8285. [[CrossRef](#)]
6. Nosaka, Y.; Nosaka, A.Y. Identification and roles of the active species generated on various photocatalysts. In *Photocatalysis and Water Purification*; Wiley-VCH Verlag GmbH & Co. KGaA: Weinheim, Germany, 2013.
7. Fujishima, A.; Zhang, X.; Tryk, D.A. TiO<sub>2</sub> photocatalysis and related surface phenomena. *Surf. Sci. Rep.* **2008**, *63*, 515–582. [[CrossRef](#)]
8. Fujishima, A.; Rao, T.N.; Tryk, D.A. Titanium dioxide photocatalysis. *J. Photochem. Photobiol. C Photochem. Rev.* **2000**, *1*, 1–21. [[CrossRef](#)]
9. Nakata, K.; Fujishima, A. TiO<sub>2</sub> photocatalysis: Design and applications. *J. Photochem. Photobiol. C Photochem. Rev.* **2012**, *13*, 169–189. [[CrossRef](#)]
10. Marugán, J.; van Grieken, R.; Pablos, C.; Satuf, M.L.; Cassano, A.E.; Alfano, O.M. Photocatalytic inactivation of escherichia coli aqueous suspensions in a fixed-bed reactor. *Catal. Today* **2015**, *252*, 143–149. [[CrossRef](#)]
11. Liu, H.-L.; Yang, T.C.-K. Photocatalytic inactivation of escherichia coli and lactobacillus helveticus by ZnO and TiO<sub>2</sub> activated with ultraviolet light. *Process Biochem.* **2003**, *39*, 475–481. [[CrossRef](#)]
12. Padervand, M.; Vossoughi, M.; Yousefi, H.; Salari, H.; Gholami, M.R. An experimental and theoretical study on the structure and photoactivity of XFe<sub>2</sub>O<sub>4</sub> (X = Mn, Fe, Ni, Co, and Zn) structures. *Russ. J. Phys. Chem. A* **2014**, *88*, 2451–2461. [[CrossRef](#)]
13. Banerjee, S.; Dionysiou, D.D.; Pillai, S.C. Self-cleaning applications of TiO<sub>2</sub> by photo-induced hydrophilicity and photocatalysis. *Appl. Catal. B Environ.* **2015**, *176–177*, 396–428. [[CrossRef](#)]
14. Klein, M.; Grabowska, E.; Zaleska, A. Noble metal modified TiO<sub>2</sub> for photocatalytic air purification. *Physicochem. Probl. Miner. Process.* **2015**, *51*, 49–57.
15. Song, J.; Wang, X.; Yan, J.; Yu, J.; Sun, G.; Ding, B. Soft Zr-doped TiO<sub>2</sub> nanofibrous membranes with enhanced photocatalytic activity for water purification. *Sci. Rep.* **2017**, *7*, 1636. [[CrossRef](#)] [[PubMed](#)]
16. Imani, R.; Dillert, R.; Bahnemann, D.W.; Pazoki, M.; Apih, T.; Kononenko, V.; Repar, N.; Kralj-Iglič, V.; Boschloo, G.; Drobne, D.; et al. Multifunctional gadolinium-doped mesoporous TiO<sub>2</sub> nanobeads: Photoluminescence, enhanced spin relaxation, and reactive oxygen species photogeneration, beneficial for cancer diagnosis and treatment. *Small* **2017**, *13*, 1–11. [[CrossRef](#)] [[PubMed](#)]
17. Seo, J.W.; Chung, H.; Kim, M.Y.; Lee, J.; Choi, I.H.; Cheon, J. Development of water-soluble single-crystalline TiO<sub>2</sub> nanoparticles for photocatalytic cancer-cell treatment. *Small* **2007**, *3*, 850–853. [[CrossRef](#)] [[PubMed](#)]
18. Ohko, Y.; Utsumi, Y.; Niwa, C.; Tatsuma, T.; Kobayakawa, K.; Satoh, Y.; Kubota, Y.; Fujishima, A. Self-sterilizing and self-cleaning of silicone catheters coated with TiO<sub>2</sub> photocatalyst thin films: A preclinical work. *J. Biomed. Mater. Res.* **2001**, *58*, 97–101. [[CrossRef](#)]

19. Suketa, N.; Sawase, T.; Kitaura, H.; Naito, M.; Baba, K.; Nakayama, K.; Wennerberg, A.; Atsuta, M. An antibacterial surface on dental implants, based on the photocatalytic bactericidal effect. *Clin. Implant Dent. Relat. Res.* **2005**, *7*, 105–111. [[CrossRef](#)] [[PubMed](#)]
20. Kim, D.S.; Kwak, S.-Y. Photocatalytic inactivation of E. coli with a mesoporous TiO<sub>2</sub> coated film using the film adhesion method. *Environ. Sci. Technol.* **2009**, *43*, 148–151. [[CrossRef](#)] [[PubMed](#)]
21. Behpour, M.; Mehrzad, M.; Hosseinpour-Mashkani, S.M. TiO<sub>2</sub> thin film: Preparation, characterization, and its photocatalytic degradation of basic yellow 28 dye. *J. Nanostructures* **2015**, *5*, 183–187.
22. Vera, M.L.; Leyva, G.; Litter, M.I. Simple TiO<sub>2</sub> coatings by sol-gel techniques combined with commercial TiO<sub>2</sub> particles for use in heterogeneous photocatalysis. *J. Nanosci. Nanotechnol.* **2017**, *17*, 4946–4954. [[CrossRef](#)]
23. Justicia, I.; Garcia, G.; Vázquez, L.; Santiso, J.; Ordejón, P.; Battiston, G.; Gerbasi, R.; Figueras, A. Self-doped titanium oxide thin films for efficient visible light photocatalysis: An example: Nonylphenol photodegradation. *Sens. Actuators B Chem.* **2005**, *109*, 52–56. [[CrossRef](#)]
24. Justicia, I.; Ordejón, P.; Canto, G.; Mozos, J.L.; Fraxedas, J.; Battiston, G.A.; Gerbasi, R.; Figueras, A. Designed self-doped titanium dioxide thin films for efficient visible-light photocatalysis. *Adv. Mater.* **2002**, *14*, 1399–1402. [[CrossRef](#)]
25. Yemmireddy, V.K.; Farrell, G.D.; Hung, Y.C. Development of titanium dioxide (TiO<sub>2</sub>) nanocoatings on food contact surfaces and method to evaluate their durability and photocatalytic bactericidal property. *J. Food Sci.* **2015**, *80*, N1903–N1911. [[CrossRef](#)] [[PubMed](#)]
26. Sopyan, I.; Watanabe, M.; Murasawa, S.; Hashimoto, K.; Fujishima, A. A film-type photocatalyst incorporating highly active TiO<sub>2</sub> powder and fluororesin binder: Photocatalytic activity and long-term stability. *J. Electroanal. Chem.* **1996**, *415*, 183–186. [[CrossRef](#)]
27. Lin, H.; Xu, Z.; Wang, X.; Long, J.; Su, W.; Fu, X.; Lin, Q. Photocatalytic and antibacterial properties of medical-grade PVC material coated with TiO<sub>2</sub> film. *J. Biomed. Mater. Res. Part B Appl. Biomater.* **2008**, *87*, 425–431. [[CrossRef](#)] [[PubMed](#)]
28. Pal, S.; Contaldi, V.; Licciulli, A.; Marzo, F. Self-cleaning mineral paint for application in architectural heritage. *Coatings* **2016**, *6*, 48. [[CrossRef](#)]
29. Gunda, N.S.K.; Singh, M.; Norman, L.; Kaur, K.; Mitra, S.K. Optimization and characterization of biomolecule immobilization on silicon substrates using (3-aminopropyl)triethoxysilane (APTES) and glutaraldehyde linker. *Appl. Surf. Sci.* **2014**, *305*, 522–530. [[CrossRef](#)]
30. Landoulsi, J.; Genet, M.J.; Kirat, K.E.; Richard, C.; Pulvin, S.; Rouxhe, P.G. Silanization with APTES for controlling the interactions between stainless steel and biocomponents: Reality vs. expectation. *Biomater. Phys. Chem.* **2011**, *5*, 99–126.
31. Li, G.; Yang, P.; Qin, W.; Maitz, M.F.; Zhou, S.; Huang, N. The effect of coimmobilizing heparin and fibronectin on titanium on hemocompatibility and endothelialization. *Biomaterials* **2011**, *32*, 4691–4703. [[CrossRef](#)] [[PubMed](#)]
32. Badv, M.; Jaffer, I.H.; Weitz, J.I.; Didar, T.F. An omniphobic lubricant-infused coating produced by chemical vapor deposition of hydrophobic organosilanes attenuates clotting on catheter surfaces. *Sci. Rep.* **2017**, *7*, 11639. [[CrossRef](#)] [[PubMed](#)]
33. Villegas, M.; Cetinic, Z.; Shakeri, A.; Didar, T.F. Fabricating smooth PDMS microfluidic channels from low-resolution 3D printed molds using an omniphobic lubricant-infused coating. *Anal. Chim. Acta* **2018**, *1000*, 248–255. [[CrossRef](#)] [[PubMed](#)]
34. Didar, T.F.; Cartwright, M.J.; Rottman, M.; Graveline, A.R.; Gamini, N.; Watters, A.L.; Leslie, D.C.; Mammoto, T.; Rodas, M.J.; Kang, J.H.; et al. Improved treatment of systemic blood infections using antibiotics with extracorporeal opsonin hemoadsorption. *Biomaterials* **2015**, *67*, 382–392. [[CrossRef](#)] [[PubMed](#)]
35. Didar, T.F.; Tabrizian, M. Generating multiplex gradients of biomolecules for controlling cellular adhesion in parallel microfluidic channels. *Lab Chip* **2012**, *12*, 4363–4371. [[CrossRef](#)] [[PubMed](#)]
36. Didar, T.F.; Bowey, K.; Almazan, G.; Tabrizian, M. A miniaturized multipurpose platform for rapid, label-free, and simultaneous separation, patterning, and in vitro culture of primary and rare cells. *Adv. Healthc. Mater.* **2014**, *3*, 253–260. [[CrossRef](#)] [[PubMed](#)]
37. Shakeri, A.; Sun, N.; Badv, M.; Didar, T.F. Generating 2-dimensional concentration gradients of biomolecules using a simple microfluidic design. *Biomicrofluidics* **2017**, *11*. [[CrossRef](#)] [[PubMed](#)]

38. Kim, W.J.; Kim, S.; Lee, B.S.; Kim, A.; Ah, C.S.; Huh, C.; Sung, G.Y.; Yun, W.S. Enhanced protein immobilization efficiency on a TiO<sub>2</sub> surface modified with a hydroxyl functional group. *Langmuir* **2009**, *25*, 11692–11697. [[CrossRef](#)] [[PubMed](#)]
39. Cheng, F.; Sajedin, S.M.; Kelly, S.M.; Lee, A.F.; Kornherr, A. UV-stable paper coated with APTES-modified P25 TiO<sub>2</sub> nanoparticles. *Carbohydr. Polym.* **2014**, *114*, 246–252. [[CrossRef](#)] [[PubMed](#)]
40. Gong, Z.; Tang, D.; Guo, Y. The fabrication and self-flocculation effect of hybrid TiO<sub>2</sub> nanoparticles grafted with poly(N-isopropylacrylamide) at ambient temperature via surface-initiated atom transfer radical polymerization. *J. Mater. Chem.* **2012**, *22*, 16872. [[CrossRef](#)]
41. Xu, Z.; Shang, J.; Liu, C.; Kang, C.; Guo, H.; Du, Y. The preparation and characterization of TiO<sub>2</sub> ultrafine particles. *Mater. Sci. Eng. B* **1999**, *63*, 211–214. [[CrossRef](#)]
42. Yu, J.-G.; Yu, H.-G.; Cheng, B.; Zhao, X.-J.; Yu, J.C.; Ho, W.-K. The effect of calcination temperature on the surface microstructure and photocatalytic activity of TiO<sub>2</sub> thin films prepared by liquid phase deposition. *J. Phys. Chem. B* **2003**, *107*, 13871–13879. [[CrossRef](#)]
43. Lopez, N.; Nørskov, J.K.; Janssens, T.V.W.; Carlsson, A.; Puig-Molina, A.; Clausen, B.S.; Grunwaldt, J.-D. The adhesion and shape of nanosized Au particles in a Au/TiO<sub>2</sub> catalyst. *J. Catal.* **2004**, *225*, 86–94. [[CrossRef](#)]
44. Kang, I.-C.; Zhang, Q.; Yin, S.; Sato, T.; Saito, F. Preparation of a visible sensitive carbon doped TiO<sub>2</sub> photo-catalyst by grinding TiO<sub>2</sub> with ethanol and heating treatment. *Appl. Catal. B Environ.* **2008**, *80*, 81–87. [[CrossRef](#)]
45. Yamada, K.; Yamane, H.; Matsushima, S.; Nakamura, H.; Ohira, K.; Kouya, M.; Kumada, K. Effect of thermal treatment on photocatalytic activity of N-doped TiO<sub>2</sub> particles under visible light. *Thin Solid Films* **2008**, *516*, 7482–7487. [[CrossRef](#)]
46. Widegren, J.; Bergström, L. The effect of acids and bases on the dispersion and stabilization of ceramic particles in ethanol. *J. Eur. Ceram. Soc.* **2000**, *20*, 659–665. [[CrossRef](#)]
47. Kardys, A.Y.; Bharali, D.J.; Mousa, S.A. Amino-functionalized silica nanoparticles: In vitro evaluation for targeted delivery and therapy of pancreatic cancer. *J. Nanotechnol.* **2013**, *2013*, 768724. [[CrossRef](#)]
48. Chen, L.-X.; Zheng, J.-N.; Wang, A.-J.; Wu, L.-J.; Chen, J.-R.; Feng, J.-J. Facile synthesis of porous bimetallic alloyed PdAg nanoflowers supported on reduced graphene oxide for simultaneous detection of ascorbic acid, dopamine, and uric acid. *Analyst* **2015**, *140*, 3183–3192. [[CrossRef](#)] [[PubMed](#)]
49. Praveen, P.; Viruthagiri, G.; Mugundan, S.; Shanmugam, N. Structural, optical and morphological analyses of pristine titanium di-oxide nanoparticles—Synthesized via sol-gel route. *Spectrochim. Acta Part A Mol. Biomol. Spectrosc.* **2014**, *117*, 622–629. [[CrossRef](#)] [[PubMed](#)]
50. Lu, H.B.; Zhou, Y.Z.; Vongehr, S.; Tang, S.C.; Meng, X.K. Effects of hydrothermal temperature on formation and decoloration characteristics of anatase TiO<sub>2</sub> nanoparticles. *Sci. China Technol. Sci.* **2012**, *55*, 894–902. [[CrossRef](#)]
51. Watson, S.; Beydoun, D.; Scott, J.; Amal, R. Preparation of nanosized crystalline TiO<sub>2</sub> particles at low temperature for photocatalysis. *J. Nanoparticle Res.* **2004**, *6*, 193–207. [[CrossRef](#)]
52. Chen, Y.F.; Lee, C.Y.; Yeng, M.Y.; Chiu, H.T. The effect of calcination temperature on the crystallinity of TiO<sub>2</sub> nanopowders. *J. Cryst. Growth* **2003**, *247*, 363–370. [[CrossRef](#)]
53. Chellappa, M.; Anjaneyulu, U.; Manivasagam, G.; Vijayalakshmi, U. Preparation and evaluation of the cytotoxic nature of TiO<sub>2</sub> nanoparticles by direct contact method. *Int. J. Nanomed.* **2015**, *10*, 31–41.
54. Socrates, G. *Infrared and Raman Characteristic Group Frequencies*, 3rd ed.; John Wiley & Sons Ltd.: Chichester, UK, 2001.
55. Olurode, K.; Neelgund, G.M.; Oki, A.; Luo, Z. A facile hydrothermal approach for construction of carbon coating on TiO<sub>2</sub> nanoparticles. *Spectrochim. Acta Part A Mol. Biomol. Spectrosc.* **2012**, *89*, 333–336. [[CrossRef](#)] [[PubMed](#)]
56. Kango, S.; Kalia, S.; Celli, A.; Njuguna, J.; Habibi, Y.; Kumar, R. Surface modification of inorganic nanoparticles for development of organic-inorganic nanocomposites—A review. *Prog. Polym. Sci.* **2013**, *38*, 1232–1261. [[CrossRef](#)]
57. Yoshimitsu, Z.; Nakajima, A.; Watanabe, T.; Hashimoto, K. Effects of surface structure on the hydrophobicity and sliding behavior of water droplets. *Langmuir* **2002**, *18*, 5818–5822. [[CrossRef](#)]
58. Han, J.-B.; Wang, X.; Wang, N.; Wei, Z.-H.; Yu, G.-P.; Zhou, Z.-G.; Wang, Q.-Q. Effect of plasma treatment on hydrophilic properties of TiO<sub>2</sub> thin films. *Surf. Coat. Technol.* **2006**, *200*, 4876–4878. [[CrossRef](#)]

59. Nie, X.; Zhuo, S.; Maeng, G.; Sohlberg, K. Doping of TiO<sub>2</sub> polymorphs for altered optical and photocatalytic properties. *Int. J. Photoenergy* **2009**, *2009*, 1–22. [[CrossRef](#)]
60. Ren, R.; Yang, Z.; Shaw, L.L. Polymorphic transformation and powder characteristics of TiO<sub>2</sub> during high energy milling. *J. Mater. Sci.* **2000**, *35*, 6015–6026. [[CrossRef](#)]
61. Mei, Z.-G.; Wang, Y.; Shang, S.; Liu, Z.-K. First-principles study of the mechanical properties and phase stability of TiO<sub>2</sub>. *Comput. Mater. Sci.* **2014**, *83*, 114–119. [[CrossRef](#)]
62. Hanaor, D.A.H.; Sorrell, C.C. Review of the anatase to rutile phase transformation. *J. Mater. Sci.* **2011**, *46*, 855–874. [[CrossRef](#)]
63. Zhao, J.; Milanova, M.; Warmoeskerken, M.M.C.G.; Dutschk, V. Surface modification of TiO<sub>2</sub> nanoparticles with silane coupling agents. *Colloids Surfaces A Physicochem. Eng. Asp.* **2012**, *413*, 273–279. [[CrossRef](#)]



© 2018 by the authors. Licensee MDPI, Basel, Switzerland. This article is an open access article distributed under the terms and conditions of the Creative Commons Attribution (CC BY) license (<http://creativecommons.org/licenses/by/4.0/>).